Phakometry and lens tilt and decentration using a custom-developed Purkinje imaging apparatus: validation and measurements

Patricia Rosales and Susana Marcos

Instituto de Optica, Consejo Superior de Investigaciones Científicas, Serrano 121, 28006 Madrid, Spain

Received April 22, 2005; revised July 27, 2005; accepted August 2, 2005

We present a Purkinje imaging system for phakometry and measurement of tilt and decentration of crystalline and intraocular lenses (IOLs). Crystalline lens radii of curvature were estimated by using both a merit function and the equivalent mirror approaches. Tilts and decentrations were estimated by using Phillips's linear analysis. We present a complete validation of the technique through exhaustive computer simulations and control experiments, and measurements in 17 normal eyes (mean age 26.67±2.31) and nine postcataract surgery eyes (mean age 74±2.3). Crystalline lens radii ranged from 12.7 to 8.81 mm and from −5.64 to −7.09 mm for anterior and posterior surfaces, respectively. Crystalline lens tilt ranged from 2.8 to −2.87 deg horizontally and from 2.58 to −1 deg vertically. Crystalline lens decentration ranged from 0.09 to 0.45 mm horizontally and from 0.09 to −0.22 mm vertically. IOL tilt ranged from 3.6 to −1.51 deg horizontally and from 5.97 to −1.85 deg vertically. IOL decentration ranged from 0.53 to −0.31 mm horizontally and from 0.13 to −0.96 mm vertically.

OCIS codes: 330.5370, 330.4300.

1. INTRODUCTION

In the last few years, there has been an increased interest in the assessment of the optical quality of the normal eye,[1,2] as well as the changes of optical quality with certain conditions such as aging,[3] accommodation,[4] or refractive errors,[5] and particularly how the optical aberrations are modified after certain interventions such as refractive surgery,[6] intraocular surgery,[7] or contact lenses.[8] While there is a good description of the ocular aberrations of the eye, driven by the development of reliable aberrometers,[9] the sources of the aberrations in individual eyes and their changes associated with different conditions are not well understood. Measurements of the corneal elevation maps allow estimation of the contribution of anterior corneal aberrations to the ocular aberrations.[10] There have been attempts to relate the presence of asymmetric aberrations such as coma to the tilt of the optical axis.[1] However, precise measurements of geometry and positioning (tilt and decentration) of the crystalline lens will allow a better understanding of the contributions of internal optics to the ocular aberrations. These data may shed light on the investigation of the accommodative mechanism of the crystalline lens, particularly on how to understand optical performance of eyes implanted with intraocular lenses (IOLs). Cataract surgery has benefited from technical advances that allow smaller corneal incisions (leading to fewer incision-induced corneal aberrations) and constant improvements of IOL design.[11] However, customization of cataract surgery will be ultimately limited by the accuracy in IOL positioning. Accurate *in vivo* measurements of IOL tilt and decentration, particularly in combination with measurements of ocular aberrations, are therefore very valuable in evaluating the actual performance of a given IOL design.

Purkinje images (reflections from anterior and posterior corneal surfaces PI and PII and from anterior and posterior crystalline lens surfaces PIII and PIV) have been used for more than a century to assess properties of the cornea and crystalline lens.

Since their description by Purkinje in 1832 Purkinje images have been widely used to obtain the power of the crystalline lens or the change of crystalline lens radii with accommodation. One of the earlier studies, by Wulfeck,[12] already describes a system to image the third Purkinje image, using infrared (IR) photography, and established the basis of the current systems. Van Veen and Goss[13] presented a Purkinje image system with a still flash camera. A similar system was used by Sorsby *et al.*[14] in their studies correlating refractive error and geometrical properties of the ocular components. Mutti *et al.*[15] employed for the first time a video camera to record the Purkinje reflections and used it to study myopia and normal ocular development in school children.[16] A telecentric stop lens (which eliminates changes in magnification when an image is defocused) was added to the video camera to record the three Purkinje images, as was used by Phillips *et al.* in a system developed to measure IOL tilt and decentration *in vivo*.[17] Several algorithms have been proposed to obtain anterior and posterior crystalline lens radii of curvature from Purkinje images. Smith and Garner[18] developed the so-called equivalent theorem mirror method, based on the replacement of the different ocular surfaces by a single mirror. The algorithm was developed for Purkinje images obtained with a system with a telecentric stop, but it also presented the corrections required in systems not provided with a telecentric lens where a change of focus is needed to image the third Purkinje image. Garner[19] proposed the alternative recursive method

called the merit function to obtain radii of curvature of the lens surfaces. This method was implemented experimentally by Barry *et al.*[20] with physical model eyes and has been used to study the change of equivalent and gradient refractive index of the crystalline lens with accommodation,[21] the changes in ocular dimensions and refraction with accommodation,[22] and the refractive index of the crystalline lens in young and aged eyes.[23]

Apart from phakometry, Purkinje images can also provide information on tilt and decentration of the ocular components and the lens in particular, which can be related to the optical quality of the eye. Several methodologies have been proposed to estimate lens tilt and decentration from Purkinje imaging systems. Several works, mainly from the clinical literature, estimate lens tilt by presenting to the subject fixation targets at different eccentricities and searching the fixation angle that produces an overlap of PIII and PIV.[24] Phillips *et al.*[17] proposed a linear relation between Purkinje image locations and rotation of the eye, tilt, and decentration of the lens in patients with IOLs. This methodology was validated and extensively used by Barry *et al.* in several studies of the misalignment of the ocular surfaces.[20,25,26]

As an alternative to Purkinje imaging, Scheimpflug imaging has also been used to study the shape of the human lens[27,28] and to measure tilt and decentration of IOLs.[29] Scheimpflug cross sections of the anterior segment of the eye provide very complete information about the shape and thickness of the lens and cornea,[30] provided that the distortions produced by refraction and the actual imaging geometry are corrected. Comparisons of measurements obtained on the same subjects with these two methods will be presented in a future work. Previous studies compared phakometry obtained from Scheimpflug imaging and magnetic resonance imaging in different groups of eyes as a function of age.[31]

Despite the fact that the use of Purkinje images to perform phakometry and to measure tilt and decentration of the lens is well known, to our knowledge the description of the practical implementation of a compact system to measure both the normal lens and intraocular lens phakometry, tilt, and decentration (in all orientations) has never been published. In addition, the performance of the system (in its actual experimental configuration) has been validated with the use of computer eye models and control experiments. The performance of the equivalent mirror theorem and merit function methods for phakometry has been assessed, in particular the limitations that arise from the fact of considering paraxial optics, spherical surfaces, or constant refractive gradient index. Models have been developed with real data obtained for individual eyes. The same eye models are used to evaluate the performance of Phillips's linear equations to obtain lens tilt and decentration. Additionally, control experiments on eyes with implanted IOLs with known nominal power allow comparisons of nominal power with the power estimated from phakometry, and comparisons with retroillumination images of the IOLs in eyes with dilated pupils allow assessment of the consistency of lens decentration estimated through Purkinje imaging.

We present measurements of crystalline lens radii of curvature as well as tilt and decentration in normal eyes and postcataract surgery eyes using the same system, showing the capabilities both for laboratory experiments and in a clinical environment.

2. METHODS

A. Purkinje Imaging Optical Setup

Figure 1 shows the optical implementation of the Purkinje imaging setup. The system is mounted on a 500×400 mm optical table. It has a symmetrical configuration for measurements on right and left eyes. The light sources are 880 nm LEDs (SFH485, Osram, 5 mm diameter, 22 deg emission angle; maximum radiant intensity 80 mW/sr). Light from LED1 and LED2 is collimated by L1 and L2 (focal length 125 mm, diameter 12.5 mm). These channels illuminate the eye at an angle of 12 deg and are used for lens tilt/decentration measurements. Double LEDs (D-LED1 and D-LED2), separated by 18 mm and mounted at a distance of 65 mm from the eye at an angle of 15 deg, were used to perform phakometry. The imaging channel consists of an IR-enhanced CCD camera (CV-M50IR, JAI) provided with a 55 mm focal length telecentric lens (Edmund Optics Ltd) mounted at a distance of 260 mm from the eye and focused at the pupil plane. This configuration resulted in a scale of 0.018 mm/pixel on the CCD chip.

A third channel projects a visual stimulus (FT) for foveal and eccentric fixations. It consists of a 12×9 mm minidisplay (Liteye Systems, pixel size 15×15 μm), subtending a visual field of 7 deg, and a Badal system to correct for refractive errors and to meet different accommodation demands. The minidisplay has Super Video Graphic Array resolution and allows presentation of multiple targets. The Badal system consists of two lenses (L3 and L4, focal length 125 mm), allowing refractive corrections ranging from −8 to 8 diopters (D).

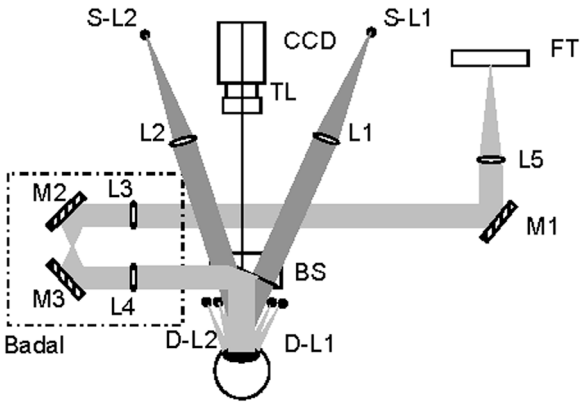

Fig. 1. Diagram of the Purkinje imaging system optical setup, with single LEDs (S-L1 and S-L2) collimated with achromatic lenses L1 and L2 ($f=125$ mm, $\phi=25$ mm) for measurements of tilt and decentration on right and left eyes, and double LEDs (D-L1 and D-L2) for phakometry. Images are captured on a CCD camera with telecentric lens (TL). Fixation targets (FT) are presented on a minidisplay, collimated by L5 ($f=125$ mm, $\phi=38$ mm) and inserted into the system with mirror M1. Illumination and imaging channels are separated by a hot mirror acting as a beam splitter (BS). A Badal system consisting of two mirrors (M2, M3) and two lenses (L3, L4) ($f=125$ mm, $\phi=25$ mm) allows for correction of refraction and for compliance with accommodative demands.

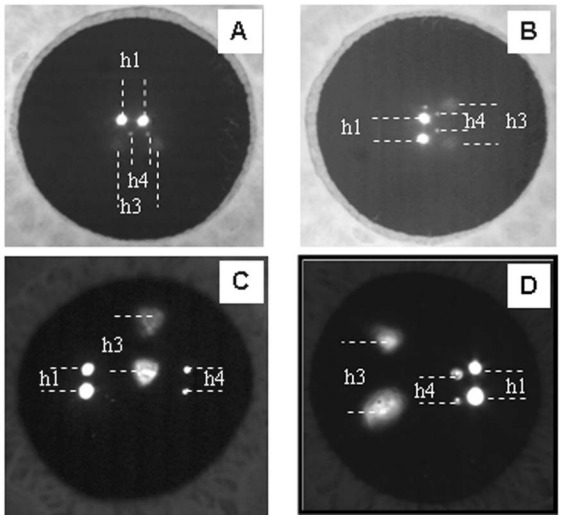

Fig. 2. Examples of pupillary images showing double PI, PIII, and PIV used to obtain phakometry: (a) eye with normal crystalline lens (eye 1, OD) in the horizontal direction, (b) eye with normal crystalline lens (eye 1, OD) in the vertical direction, (c) eye with IOL (eye 2, OS), (d) eye with IOL (eye 2, OS).

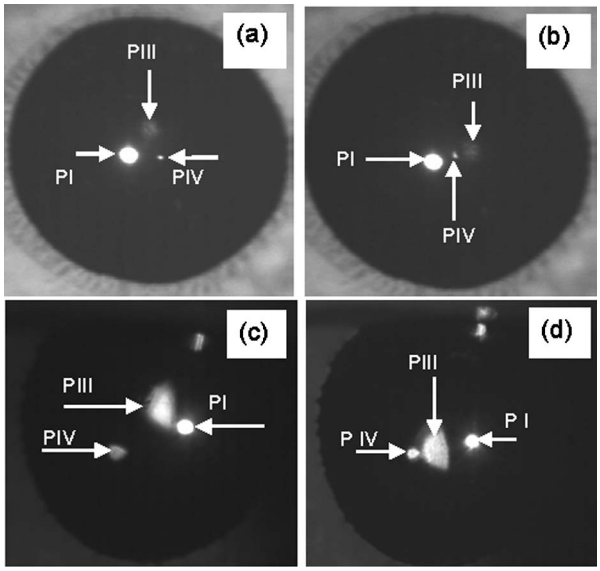

Fig. 3. Examples of pupillary images showing PI, PIII, and PIV used to obtain tilt and decentration for different fixation angles: (a) eye with normal crystalline lens (subject 15, OD) fixating at −3.5 deg temporal, (b) eye with normal crystalline lens (subject 15, OD) fixating at 3.5 deg inferior, (c) eye with IOL (eye 2, OS) fixating at 1.7 deg superior, (d) eye with IOL (eye 2, OS) fixating at 1.7 deg inferior.

The system is controlled automatically with software written in Visual Basic (Microsoft Visual Studio, 6.0). The Windows-based program incorporates capture of pupillary images (by means of an acquisition board), LED switch on and off, presentation of targets on the system's minidisplay (with a simultaneous view of the target on the controlling program), and patient data handling.

B. Experimental Protocol

Subjects are aligned to the system while looking foveally at a fixation cross target presented on the minidisplay. The subject's pupil is aligned to the optical axis of the CCD camera while moving the subject's head on an *X–Y–Z* stage. The subject's head is stabilized by means of a dental impression. Spherical refractive error is corrected with the Badal system, which was set in the position for which the subject reported that the stimulus looked sharpest. In subjects with accommodative capability, special care was taken to ensure that the eye was not accommodating. Measurements were typically done under normal viewing conditions in the young eyes and mydriasis (tropicamide 1%) in patients with IOLs.

A set of pupillary images showing PI, PIII, and PIV are captured, with SL1 (for OD) or SL2 (for OS) on, for ten different fixations on the minidisplay (green spots on a black background). Fixation locations ranged from +3.5 to −3.5 deg in the horizontal direction and from +2.5 to −2.5 deg in the vertical direction. These images were used for estimations of lens tilt and decentration. We captured three sets of images for statistical purposes.

Pupillary images showing double PI, PIII, and PIV are also captured with D-LED1 (for OD) or D-LED2 (for OS) on, with the patient fixating foveally. Occasionally, the fixation target had to be moved off axis to allow proper visualization of the images (a special module in the software allows easy shift and documentation of the fixation location). These images were used for estimations of lens radii of curvature. We captured three sets of images (for vertical and horizontal directions) for statistical purposes.

Figure 2 shows typical images for phakometry obtained in normal eyes and patients with IOLs. Figure 3 shows typical images used to estimate tilt and decentration in normal eyes and in patients with IOLs.

Additional measurements on the subjects included corneal topography (Atlas, Humphrey Instruments) axial length, anterior chamber depth and keratometry (IOL Master, Zeiss), and autorefraction (Automatic Refractor Model 597, Zeiss). IR (780 nm) retroillumination images (from a pupil imaging channel in the Laser Ray Tracing system developed in our laboratory)[32] were also captured in patients with implanted IOLs.

C. Purkinje Image Processing

We estimate the location of the Purkinje images referred to the pupil center. The center of the pupil is estimated by detection of the pupil margin, which is fitted to a circle. The position of the Purkinje images obtained from the reflection of the single LED on the different ocular surfaces, referred to the pupil center, is detected through a Gaussian fitting, with routines written in Matlab.

D. Phakometry

We implemented two methods, the equivalent mirror method and a merit function, proposed by Garner[19] and by Smith and Garner,[18] respectively, to obtain the anterior and posterior radii of curvature from the Purkinje images of double LEDs. A detailed description of the methods can be found elsewhere.[18,19] In brief, the equivalent mirror theorem establishes that different dioptric surfaces followed by a catoptric surface can be replaced by a single mirror with an equivalent radius of curvature. The theorem is applied twice: (1) for the anterior lens, anterior and posterior corneal surfaces and anterior lens surfaces

are replaced by a single mirror with an equivalent radius of curvature; and (2) for the posterior lens, anterior and posterior corneal surfaces and anterior and posterior lens surfaces are replaced by a single mirror with an equivalent radius of curvature.

Garner's merit function[33] (f_3 and f_4) is given by

$$f_3 = \left[\left(\frac{h_3}{h_1}\right)_{\text{th}}\right]^2 - \left[\left(\frac{h_3}{h_1}\right)_{\text{exp}}\right]^2,$$

$$f_4 = \left[\left(\frac{h_4}{h_1}\right)_{\text{th}}\right]^2 - \left[\left(\frac{h_4}{h_1}\right)_{\text{exp}}\right]^2. \quad (1)$$

Input values are the experimental heights of the double PIII relative to double PI $(h_3/h_1)_{\text{exp}}$ and experimental heights of the double PIV relative to double PI $(h_4/h_1)_{\text{exp}}$ Theoretical relative heights [$(h_3/h_1)_{\text{th}}$ and $(h_4/h_1)_{\text{th}}$] are obtained recursively by simulating a ray tracing through the different ocular surfaces assuming starting values for anterior and posterior lens radii of curvatures. Ray tracing, as well as the standard minimization routines, was programmed in Matlab.

E. Lens Tilt and Decentration

The method to obtain lens tilt and decentration is based on that described by Phillips *et al.*[17] and Barry *et al.*[20] in previous works. This method assumes a linear relation between Purkinje image positions and rotation of the eye, tilt, and decentration:

$$P1 = E\beta,$$

$$P3 = F\beta + A\alpha + Cd,$$

$$P4 = G\beta + B\alpha + Dd, \quad (2)$$

where P1, P3, and P4 are the Purkinje image positions referred to the pupil center and β, α, and d are the rotation angle of the eye, tilt, and decentration of the lens, respectively. These equations are applied to both horizontal and vertical coordinates.

To obtain the coefficients in these equations for each eye, we resort to simulated model eyes with spherical surfaces and the individual parameters available for each subject, using an optical design program (Zemax, Focus Software). The anterior corneal radius and anterior chamber depth were obtained from optical biometry, and anterior and posterior lens radii of curvatures were obtained from the phakometry measurements. Corneal thickness, lens thickness, and lens refractive index were taken constant in all eyes, using data from the unaccommodated Gullstrand model eye. IOL parameters (index of refraction $n=1.46$ and thickness 1.164 mm) were obtained from published data on these lenses.[34] Indices of refraction for the wavelength of illumination were used, with conversion factors reported by the Herzberger formula[35] given by

$$n = a + bL + cL^2 + d\lambda^2 + e\lambda^4 + f\lambda^6, \quad (3)$$

where $L=1/(\lambda^2-0.028)$ and a, b, c, d, e, and f are the dispersion coefficient data of the corresponding media provided by Zemax.

The optical surfaces were assumed to be spherical, although validations of the technique were performed incorporating aspheric surfaces, actual corneal topographies, and gradient index of refraction into the models.

To obtain coefficients E, F, and G, in Eqs. (2), we set $\alpha=0$ and $d=0$ (no tilt and no decentration) in the model, estimated the Purkinje image positions for different rotation angles, and calculated coefficients E, F, and G by linear fitting of the slope. The same procedure was repeated for A and B (setting $\beta=0$ and $d=0$) and C and D (with $\beta=0$ and $\alpha=0$).

The rotation angle (β), tilt (α), and decentration of the lens (d) can then be solved by using the individual coefficients for each eye and the experimental Purkinje image locations ($P1$, $P3$, and $P4$):

$$\beta = \frac{P1}{E},$$

$$\alpha = \frac{\beta(DF - CG) + CP4 - DP3}{CB - DA},$$

$$d = \frac{P3 - \beta F - \alpha A}{C}. \quad (4)$$

F. Subjects

Measurements were made on 17 eyes from normal subjects, moderately myopic with spherical errors ranging from 1.25 to −7 D (mean=−1.71±2.39 D) and ages ranging from 24 to 30 yr (mean=26.67±2.31 yr). Additionally, we measured nine eyes of five subjects implanted with IOLs (with both aspheric and spherical designs), with ages ranging from 71 to 79 yr (mean=74±2.3 yr). All subjects were informed of the nature of the study before the experiments and signed a consent form. The study followed the tenets of the declaration of Helsinki.

3. RESULTS

A. Control Experiments and Simulations

We performed computer simulations to test individually the validity of the assumptions involved in the described procedures. Additionally, measurements in patients with IOLs allowed us to performed comparisons with nominal values and comparisons with other methods.

1. Test of Phakometry Methods Using Computer Eye Models

We performed computer simulations to test the performance of the equivalent mirror and merit function approaches to obtain phakometry. Simulations are based on the same simplified eye model (spherical surfaces, constant refractive index) as the model that we used in the processing algorithms. Table 1 shows the parameters of the eye model used in the simulation, as well as the individual parameter that was varied in each case to test separately the impact of each of the assumptions. All simulations were performed in Zemax, using the actual experimental conditions for illumination (double LED, distance from the LED to the eye, and angle of illumina-

tion). The actual images of PI, PII, and PIII were obtained by using ray tracing and intensity distribution analysis in Zemax. As in the experiments, the locations of the double Purkinje images of PI, PII, and PIII were obtained by fitting Gaussian functions to the images. From those locations, we computed the relative heights. We used these values in the same algorithms that processed our experimental data and compared the resultant radii of curvature with the nominal values from the eye model. Table 1 shows the retrieved anterior and posterior lens radii of curvature for different combinations of anterior and posterior nominal lens radii of curvature in the model eye. For eyes with anterior lens radii ranging from 14 to 10 mm, we found average discrepancies of 0.09 mm for the anterior lens and 1.12 mm for the posterior lens with the equivalent mirror method and 0.09 mm for the anterior lens and 0.33 mm for the posterior lens with the merit function method. For eyes with posterior lens radii ranging from −4 to −6 mm, we found average discrepancies of 1.06 and 0.30 mm in the retrieved posterior lens radius with the merit function and equivalent mirror methods, respectively.

Alternatively, we compared the experimental heights of the Purkinje images with those obtained through simulations in Zemax using the experimentally retrieved values of anterior and posterior lens radii of curvatures. We found average discrepancies of 0.009 mm for h_1, 0.131 mm for h_3, and 0.002 mm for h_4. These discrepancies in Purkinje image heights obtained experimentally and with simulations in Zemax, translated into radii of curvature differences of 0.366 and 0.075 mm for the anterior lens (with the equivalent mirror method and the merit function, respectively) and 1.09 and 0.217 mm for the posterior lens. The discrepancies in h_1, h_3, and h_4 are close to the distance measurement accuracy (taking into account that a pixel resolution is 0.08 mm at the pupil plane).

We also performed simulations to assess the influence of possible tilt and decentration of the lens, corneal curvature, anterior chamber depth, and lens thickness on the phakometry measurements.

Effect of lens tilt and decentration. To evaluate possible effects of misalignment of the lens on the estimates of lens radii of curvature, we simulated the same model eye with the parameters shown in Table 1 and a decentered and tilted lens. We obtained a discrepancy of 0.28 mm for the anterior lens and 1.55 mm for the posterior lens with the equivalent mirror method and of 0.66 mm for the anterior lens and 0.46 mm for the posterior lens with the merit function method.

Effect of anterior and posterior corneal curvature. We checked that the estimates were not affected by the nominal corneal curvatures. The anterior corneal radius was changed in the processing algorithm according to the nominal value of the model, while the posterior corneal radius was always kept constant in the processing algorithm. For the values of the eye model shown in Table 1, and varying the anterior corneal curvature, we found average discrepancies of 0.12 and 0.29 mm for the retrieved anterior lens radius and of 1.02 and 0.21 mm for the retrieved posterior lens radius, using the equivalent mirror and merit function methods, respectively. For the fixed values of the model shown in Table 1, and varying the posterior corneal curvature, we found average discrepan-

Table 1. Model Eye with Spherical Surfaces (n_{cornea}=1.3687, n_{lens}=1.41, n_{aqueous}=1.32854) for 880 nm in Zemax with Herzberger Formula [Eq. (3)]

Eye Model Nominal Values								Retrieved Values: Equivalent Mirror		Retrieved Values: Merit Function	
Anterior Corneal Radius (mm)	Posterior Corneal Radius (mm)	Anterior Chamber Depth (mm)	Lens Thickness (mm)	Lens Decentration (mm)	Lens Tilt (deg)	Anterior Lens Radius (mm)	Posterior Lens Radius (mm)	Anterior Lens Radius (mm)	Posterior Lens Radius (mm)	Anterior Lens Radius (mm)	Posterior Lens Radius (mm)
7.73	6.5	3.61	4	0	0	**10**	−6	10.15	−7.35	9.96	−6.51
7.73	6.5	3.61	4	0	0	**12**	−6	12.13	−7.04	11.94	−6.27
7.73	6.5	3.61	4	0	0	**14**	−6	13.99	−7.35	13.80	−6.53
7.73	6.5	3.61	4	0	0	10.45	**−6**	10.68	−7.12	10.32	−6.15
7.73	6.5	3.61	4	0	0	10.45	**−5**	10.68	−6.03	10.32	−5.28
7.73	6.5	3.61	4	0	0	10.45	**−4**	10.68	−5.06	10.32	−4.48
7.73	6.5	3.61	4	**1**	**5**	10.45	−6	10.18	−7.55	9.79	−6.46
8.5	6.5	3.61	4	0	0	10.45	−6	10.49	−7.03	10.23	−6.19
7.5	6.5	3.61	4	0	0	10.45	−6	10.55	−7.16	10.14	−6.14
6.5	6.5	3.61	4	0	0	10.45	−6	10.69	−6.88	10.08	−5.69
7.73	**6.5**	3.61	4	0	0	10.45	−6	10.56	−7.24	10.19	−6.24
7.73	**6**	3.61	4	0	0	10.45	−6	10.57	−7.21	10.19	−6.22
7.73	**5.5**	3.61	4	0	0	10.45	−6	10.48	−6.97	10.11	−6.03
7.73	6.5	**4**	**4**	0	0	10.45	−6	10.92	−7.52	10.54	−6.47
7.73	6.5	**3.5**	**4**	0	0	10.45	−6	10.58	−7.27	10.21	−6.27
7.73	6.5	**2**	**4**	0	0	10.45	−6	10.57	−7.19	10.19	−6.26
7.73	6.5	3.61	**3**	0	0	10.45	−6	10.7	−5.91	10.84	−5.17
7.73	6.5	3.61	**3.5**	0	0	10.45	−6	10.7	−6.64	10.84	−5.75
7.73	6.5	3.61	**4**	0	0	10.45	−6	10.7	−6.97	10.84	−6

Table 2. Realistic Model Eye with Aspheric Surfaces, Anterior Corneal Elevation from Corneal Topography, Gradient Refractive Index in the Lens, and Lens Tilt and Decentration

Eye Model Nominal Values													Retrieved Values			
Anterior Corneal			Posterior Corneal		Anterior Lens		Lens Refractive Index (IR)[c]		Posterior Lens				Equivalent Mirror		Merit Function	
Radius (mm)	Aspher.[a]	rms[b]	Radius (mm)	Aspher.	Radius (mm)	Aspher.	Const.	Grad. (equiv. index)	Tilt	Decen.	Radius (mm)	Aspher.	Anterior Lens Radius (mm)	Posterior Lens Radius (mm)	Anterior Lens Radius (mm)	Posterior Lens Radius (mm)
7.73	**−0.5**	0	6.5	−0.28	10.45	0	1.41	0	0	0	−6	0	10.39	−6.99	10.03	−6.04
7.73	**−0.3**	0	6.5	−0.28	10.45	0	1.41	0	0	0	−6	0	10.39	−7.06	10.03	−6.10
7.73	**−0.2**	0	6.5	−0.28	10.45	0	1.41	0	0	0	−6	0	10.61	−7.37	10.24	−6.34
7.73	—	0.84	6.5	−0.28	10.28	0	1.41	0	0	0	−6.53	0	10.82	−7.11	10.45	−6.14
7.84	—	0.42	6.5	−0.28	11.95	0	1.41	0	0	0	−5.75	0	11.32	−6.97	11.82	−6.04
7.73	0	0	6.5	0	10.45	**−5**	1.41	0	0	0	−6	−3.25	11.14	−8.25	10.76	−7.03
7.73	0	0	6.5	0	10.45	**−3**	1.41	0	0	0	−6	−3.25	10.94	−8.28	10.56	−7.05
7.73	0	0	6.5	0	10.45	**−2**	1.41	0	0	0	−6	−3.25	10.89	−8.06	10.52	−6.88
7.73	0	0	6.5	0	10.45	−4.25	1.41	0	0	0	−6	**−3**	11.28	−8.3	10.89	−7.07
7.73	0	0	6.5	0	10.45	−4.25	1.41	0	0	0	−6	**−2**	11.28	−7.72	10.89	−6.62
7.73	0	0	6.5	0	10.45	−4.25	1.41	0	0	0	−6	**−1**	11.28	−7.51	10.89	−6.46
7.73	—	0.84	6.5	−0.28	10.28	−4.25	0	1.425	0	0	−6.53	−3.25	12.59	−8.25	10.93	−7
7.84	—	0.42	6.5	−0.28	11.95	−4.25	0	1.419	0	0	−5.75	−3.25	13	−7.84	12.59	−6.69
7.73	—	0.84	6.5	−0.28	10.28	−4.25	0	1.425	**5**	**1**	−6.53	−3.25	11.53	−8.06	11.12	−6.86

[a]Asphericity defined for this surface is $h^2+(1+Q)Z^2-2ZR=0$, where the Z axis is the optical axis, $h^2=X^2+Y^2$, R is the vertex radius of curvature, and Q is the surface asphericity.

[b]Third- and higher-order corneal surface rms (fitted to a seventh-order Zernike polynomial), without spherical terms c_{12} and c_{24}.

[c]Equivalent refractive index: gradient index (GRIN) profile in the equatorial plane defined by Garner *et al.*[23] $n(y)=n_c+c_1(y/b)^2$, where $n_c=1.406$ is the refractive index in the center of the lens, b is the equatorial radius, and c_1 is the GRIN shape factor.

cies of 0.43 and 0.29 mm in the retrieved anterior lens radius with the equivalent mirror and merit function methods, respectively. For the posterior lens radius, we found discrepancies of 1.14 and 0.16 mm with the equivalent mirror and merit function methods, respectively.

Effect of anterior chamber depth. When the anterior chamber depth was varied in a range consistent with values measured in real eyes (see Table 1), we found average discrepancies of 0.24 and 0.19 mm for the retrieved anterior lens radius and of 1.33 and 0.33 mm for the retrieved posterior lens radius, using the equivalent mirror and merit function methods, respectively. Additionally, we tested that discrepancies of 0.5 mm between the anterior chamber depth used in the model eye and that used in the simulation produced average discrepancies of 0.4 and 0.026 mm for the retrieved anterior lens radius and of 1.46 and 0.41 mm for the retrieved posterior lens radius, using the equivalent mirror and merit function methods, respectively.

Effect of lens thickness. We tested the effect of the assumption of a constant value for lens thickness, changing this parameter in the model eye (see Table 1) while keeping it constant in the processing algorithms. We found that discrepancies of 0.5 mm between the lens thickness value used in the model eye and that used in the simulation produced average discrepancies of 0.36 and 0.56 mm for the retrieved posterior lens radius with the equivalent mirror and merit function methods, respectively.

In summary, for the anterior lens radius, both methods work theoretically within accuracies <0.3 mm, and for the posterior lens radius the accuracies are within 1 mm for the equivalent mirror method and 0.3 mm for the merit function method. The estimates are not significantly affected by the assumptions regarding posterior corneal radius and lens thickness, in particular when using the merit function method.

In brief, these simulations show that, assuming spherical surfaces and for the experimental conditions of the system, the merit function provides accurate estimates of phakometry while the equivalent mirror theorem slightly overestimates the posterior lens radius.

2. Test of Phakometry Methods from Comparisons of Nominal and Experimental Intraocular Lens Power

Phakometry measurements in eyes with implanted IOLs allowed us to perform comparisons between the nominal IOL power (from the specifications of the lens) and the power estimated from the experimental IOL radii of curvature using the lensmaker formula

$$P = P_{a\_lens} + P_{p\_lens} - \frac{(D \cdot P_{a\_lens} \cdot P_{p\_lens})}{n_L}, \qquad (5)$$

where D is the IOL thickness (1.146 mm), and P_{a_lens} and P_{p_lens} are, respectively, the anterior and posterior IOL powers.

Nominal IOL power ranged from 19.5 to 24 D. We found an average power discrepancy of 0.77 D when using the equivalent mirror method and of 1.05 D when using the merit function. On an individual basis, there was not a clear tendency for one method to produce closer results to the nominal values than the other, nor a correlation of the discrepancy with IOL-related parameters (power or surface geometry).

3. Test of Lens Tilt/Decentration Methods Using Computer Eye Models

We performed computer simulations to check the accuracy of the Phillips equations—retrieving tilts and decentrations. We built a computer model with nominal values as in Table 1 (row 7), imposing crystalline lens tilts and decentration. Different combinations of tilt and decentration were also tested (with eye rotations up to 3.5 deg, lens tilts up to 5 deg, and decentrations up to 0.25 mm). We estimated the coefficients of Eqs. (2) for the model eye as described in Subsection 2.E for real eyes. Intensity distributions for Purkinje images PI, PIII, and PIV were simulated as described above, for the actual experimental conditions of eye rotation and angle of illumination, and P1, P3, and P4 in Eqs. (2) were estimated as in the experimental images. Eye rotation, tilt, and decentrations were obtained, as described for real eyes, by using Eq. (3). We found maximum discrepancies of 0.1 deg in eye rotation, 0.6 deg in lens tilt, and 0.026 mm in decentration.

Using similar procedures, we simulated P1, P3, and P4 for measured values of anterior corneal radii of curvature, anterior and posterior crystalline lens radii of curvature, and anterior chamber depth in one of the measured patients and compared experimental locations of the Purkinje images with the predictions from Zemax. We found average discrepancies of 0.058 mm for P1 in the horizontal direction and 0.024 mm in the vertical direction, 0.024 mm for P3 in the horizontal direction and 0.03 mm in the vertical direction, and 0.058 mm for P4 in the horizontal direction and 0.02 mm in the vertical direction.

Finally, we tested that discrepancies of 1 mm in the estimated anterior and posterior radii of curvature produced discrepancies of less than 0.2 deg in the tilt estimates and 0.01 mm in the decentration estimates.

4. Test of Lens Decentration Methods from Comparisons with Data from Retroillumination Techniques

IR retroillumination pupillary images showed, at least partially, the edge of the IOLs in several patients with implanted IOLs. We were able to estimate the center of the IOL with respect to the center of the dilated pupil in three eyes of the nine patients by fitting a circle to the visible IOL margins. Direct measurements of lens decentration were compared with decentrations estimated from the Purkinje images. This test allowed us to estimate if the magnitude of tilt and decentration measured with the Purkinje imaging system was consistent with the IOL position measured directly and also to validate the sign criteria. We found very good agreement between both types of measurements, with average differences of 0.03 ± 0.03 mm for decentrations in the horizontal direction and of 0.09 ± 0.03 mm for those in the vertical direction.

5. Test of the Validity of the Assumptions in the Model Eye

The computer simulations presented in Table 1 were aimed at testing the validity of the procedures with the

actual experimental conditions but used simplified eye models with spherical surfaces and constant refractive index. We have performed additional simulations to test the impact of these assumptions on the estimated lens radii of curvature and lens tilt and decentration. The parameters of the model in each condition and the results are presented in Table 2. Purkinje images were simulated by using more realistic eye models, while phakometry and lens tilt and decentrations were obtained by using the same routines as those in previous simulations and in the experiments. Implicitly these tests also checked the validity of the paraxial approximation.

Effect of anterior corneal asphericity. We assumed the same eye model as that in previous simulations but with anterior corneal conic constants consistent with reports from Dubbelman *et al.*[30] (see Table 2). The retrieved anterior lens radii differed from nominal values by 0.09 and 0.35 mm with the equivalent mirror and merit function methods, respectively, and the posterior lens radii differed by 0.94 and 0.13 mm, respectively.

Effect of corneal irregularities. We replaced the theoretical cornea in the model eye by the corneal elevation obtained with the corneal topographer in two real eyes (fitted to a seventh-order Zernike polynomial and described in Table 2 in terms of third- and higher-order root mean square errors, excluding spherical terms). We found average discrepancies of 0.59 and 0.15 mm for the retrieved anterior lens radius and 0.9 and 0.35 mm for the retrieved posterior lens radius, using the equivalent mirror and merit function methods, respectively.

Effect of anterior and posterior lens asphericities. We used the same eye model as that in previous simulations but assuming lens asphericities consistent with reports from Dubbelman and van der Heijde,[27] as shown in Table 2. When the lens anterior surface asphericity was varied, we found that the estimates of anterior lens radii are only slightly affected by changes in anterior lens asphericity (average discrepancies of 0.54 and 0.16 mm with the equivalent mirror and merit function methods, respectively) but that discrepancies in posterior lens radii are higher (average discrepancies of 2.19 and 0.98 mm with the equivalent mirror and merit function methods, respectively). The average discrepancies in the posterior lens radii (changing the posterior lens asphericity) were 2.3 and 1.07 mm with the equivalent mirror and merit function methods, respectively. These simulations show that the merit function method is more robust to the presence of aspheric surfaces and provides significantly better results than does the equivalent mirror method.

Effect of refractive gradient index in a realistic eye model. Finally, we tested the accuracy of the phakometry methods and tilt/decentration estimates by using the realistic eye model described in rows 12 and 13 of Table 2. This included real anterior corneal elevation from corneal topography, aspheric posterior corneal surfaces, anterior and posterior aspheric lens surfaces, and, particularly, a gradient index distribution for the crystalline lens (based on the model proposed by Garner and Smith[21]). With this model eye, we found a discrepancy of 0.85 and 0.66 mm for the retrieved anterior lens radius and of 1.35 and 0.75 mm for the retrieved posterior lens radius with the equivalent mirror and merit function methods, respectively. These values are only slightly higher than the discrepancies obtained by using the same eye model (with spherical surfaces and constant index of refraction) in the simulations and in the reconstruction algorithms.

We also checked that the approximations of the model did not affect the results of lens tilt and decentration. The coefficients in Phillips's equation changed by 8% on average between using the spherical model eye and the more realistic model eyes described above. These differences produced differences between the estimates lower than 0.09 and 0.01 deg for horizontal and vertical tilt, respectively, and lower than 0.16 and 0.02 for horizontal and vertical decentration, respectively, for the same nominal tilts and decentrations as those used in Subsection 3.A.3. Finally, using the same procedures as those described in Subsection 3.A.3, we simulated Purkinje images for a given tilt and decentration of the crystalline lens in the realistic eye model described above and compared the nominal values with those obtained with the algorithms. We found maximum discrepancies of 0.1 deg in eye rotation, 0.25 deg in lens tilt, and 0.013 mm in decentration. Those discrepancies are comparable with those obtained in Subsection 3.A.3, where the simulations were performed using the same spherical eye model used in the processing algorithms.

B. Phakometry in Normal Eyes

Figure 4 shows the anterior and posterior radii of curvature for 12 subjects. Radii of curvature of the anterior lens surface ranged from 8.81 to 12.69 mm, and radii of curvature of the posterior lens ranged from −7.09 to −5.64 mm, with use of the merit function method. The equivalent mirror method yielded similar radii for the anterior lens (ranging from 8.83 to 12.86 mm) and slightly overestimated values for the posterior lens (ranging from −8.43 to −6.47 mm), consistent with the predictions from the simulations.

We measured radii of curvature in the vertical and in the horizontal directions in five subjects. Differences across meridians were not significant, except for two subjects, where we found differences of 0.82 mm for the anterior lens and 0.84 mm for the posterior lens across meridians.

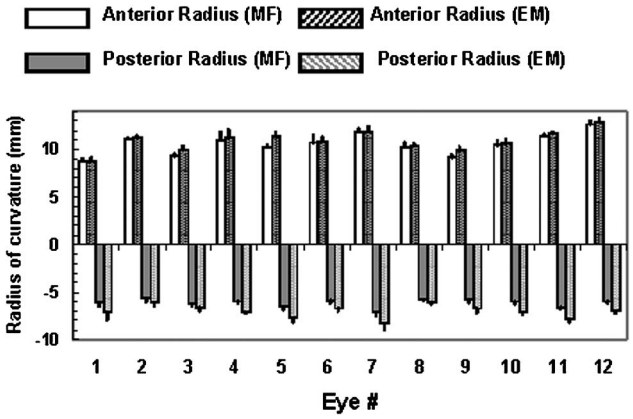

Fig. 4. Anterior and posterior radii of curvature, estimated by using the merit function (MF) and equivalent mirror (EM) methods. Eyes (right eyes from 12 subjects) are ranked by increased myopic error. Values are an average of at least three measurements. Error bars stand for standard deviations.

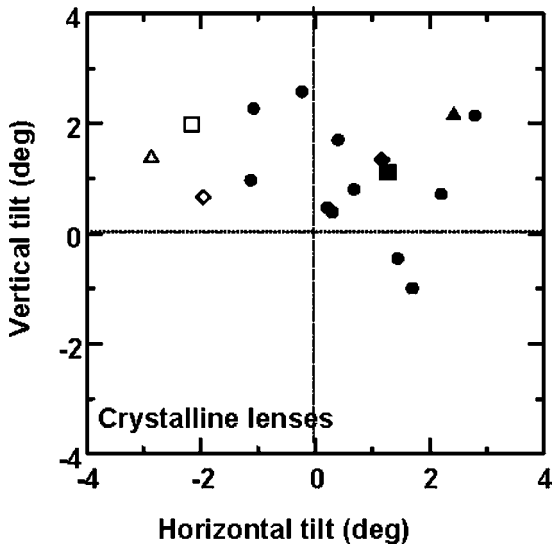

Fig. 5. Horizontal and vertical tilt of the crystalline lens in 17 eyes of 14 subjects. Solid symbols correspond to right eyes, and open symbols to left eyes. Circles correspond to subjects 1–11; squares, triangles, and diamonds to subjects 12, 13, and 14, respectively. Horizontal tilts represent tilts about the y axis, and vertical tilts those about the x axis. Error bars are smaller than the symbol size.

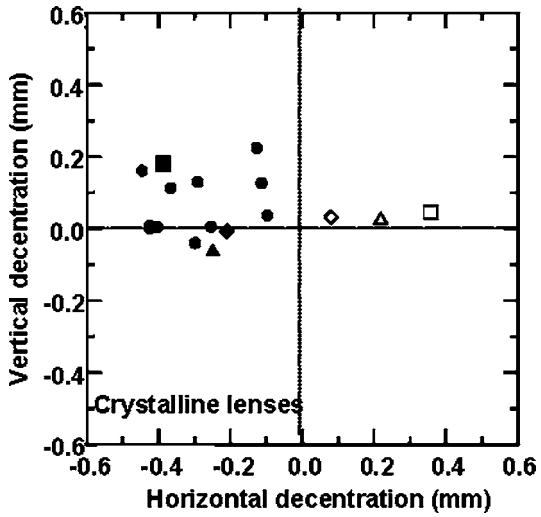

Fig. 6. Horizontal and vertical decentration of the crystalline lens in 17 eyes of 14 subjects. Solid symbols correspond to right eyes, and open symbols to left eyes, labeled as in Fig. 5. Positive horizontal decentrations represent temporal shifts from the pupil center for the right eye, and nasal shifts for the left eyes. Error bars are smaller than the symbol size.

C. Crystalline Lens Tilt and Decentration

Figure 5 shows horizontal and vertical crystalline lens tilt, and Fig. 6 shows horizontal and vertical crystalline lens decentration on 17 eyes of 14 subjects. Solid symbols stand for right eyes, and open symbols for left eyes.

Horizontal tilt refers to tilt about the y axis, and vertical tilt refers to tilt about the x axis. Positive horizontal tilt indicates that the nasal edge of the lens moves backward, and negative horizontal tilt means that the nasal edge of the lens moves forward. Positive vertical tilt indicates that the superior edge of the lens is closer to the cornea than the inferior edge, and vice versa for negative vertical tilt. Positive horizontal decentration indicates that the lens is shifted toward the temporal direction, and negative horizontal decentration indicates that the lens is shifted toward the nasal direction, for the right eye, and vice versa for the left eye. Positive vertical decentration means that the lens is shifted upward, and negative vertical decentration means that the lens is shifted downward.

Horizontal tilt ranged from −1.13 to 2.8 deg in right eyes and from −1.96 to −2.87 deg in left eyes. Vertical tilt ranged from −1 to 2.58 deg in right eyes and from 0.66 to 1.99 deg in left eyes. Crystalline lens tilt tended to be mirror-symmetric in left/right eyes of the same subject. Crystalline lens decentrations ranged, in the horizontal direction, from 0.098 to 0.445 mm in right eyes and from −0.36 to 0.39 mm in left eyes. Vertical decentrations ranged from −0.22 to 0.04 mm in right eyes and from −0.18 to 0.06 mm in left eyes.

D. Intraocular Lens Tilt and Decentration

Figure 7 shows IOL tilt, and Fig. 8 shows decentration, in eight eyes of five subjects. The sign convention is the same as that for the crystalline lens. IOL horizontal tilt ranged from −0.72 to −3.6 deg in right eyes and from −1.51 to 3.48 deg in left eyes. Vertical tilt ranged from −1.85 to 5.97 deg in right eyes and from 0.75 to 3.83 deg in left eyes. IOL decentrations ranged, in the horizontal direction, from −0.31 to 0.53 mm in right eyes and from 0.23 to 0.51 mm in left eyes. Vertical decentrations ranged from −0.96 to 0.13 mm in right eyes and from −0.96 to −0.33 mm in left eyes.

4. DISCUSSION

A. Comparison with Previous Studies

There is extensive literature presenting phakometry data. However, very few studies present a detailed analy-

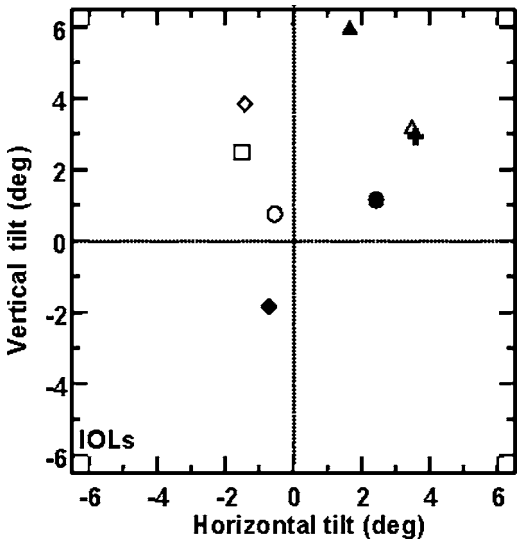

Fig. 7. Horizontal and vertical tilt of the IOL in eight eyes of five subjects after cataract surgery. Solid symbols correspond to right eyes and spherical IOLs, and open symbols correspond to left eyes and aspheric IOLs. Each shape correspond to a different subject. Signs are as in Fig. 5. Error bars are smaller than the symbol size.

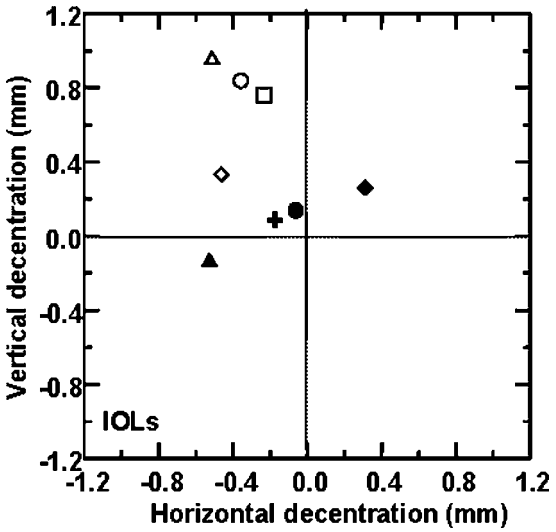

Fig. 8. Horizontal and vertical decentration of the IOL in eight eyes of five subjects after cataract surgery. Solid symbols correspond to right eyes, and spherical IOLs, and open symbols correspond to left eyes and aspheric IOLs. Each shape corresponds to a different subject. Signs are as in Fig. 5. Error bars are smaller than the symbol size.

sis of the accuracy of the technique used, which prevents judging the correctness of the lens radii of curvature on an individual basis.

Most of the very early studies with Purkinje imaging did not use individual biometric data of the eyes under test, and based their computations on the equivalent mirror theorem, which we have shown in this study to overestimate the posterior radius of curvature. Also, many of these data did not incorporate corrections of parallax errors induced by conventional lenses, which were later proposed by Smith and Garner.[18] Mutti *et al.*[15] were the first to introduce a video camera in a Purkinje imaging system and to conduct systematic phakometry measurements (in a pediatric population). The experimental protocols were complicated by the necessity of moving the focal plane to capture PIII[15] and the use of visible light, which caused photophobia in some of the subjects. Phillips suggested for the first time the use of a telecentric lens to obtain the three Purkinje images on the same plane.[17] Barry *et al.*[20] presented a Purkinje-image-based system to perform phakometry and to determine tilt and decentration of the crystalline lens in the accommodated and relaxed eye.[26] They validated the system with physical model eyes[36] and studied the accuracy of the ray tracing technique.[25,37]

We have built up a new system, suited for phakometry/positioning measurements of both the crystalline lens and IOLs. The instrument is very compact and well adapted to clinical use. The incorporation of a Badal system and flexible fixation targets can ensure relaxed accommodation. Also, a thorough validation has been performed, using both realistic simulations of the actual intensity distributions of PI, PIII, and PIV in the pupillary image, and for the first time, to our knowledge, tilt and decentration data were published in both the horizontal and vertical directions.

Our analysis shows that the merit function provides more accurate data than does the equivalent mirror theorem. Our average phakometry results using the merit function method (10.61 ± 1.13 and -6.15 ± 0.41 mm for the anterior and posterior lens, respectively) can be compared with those reported by other authors. Kirschkamp *et al.*,[26] using the Purkinje image system of Barry *et al.*[20] and the equivalent mirror, reported for the unaccommodated eye ($n=9$ with age ranging from 20 to 38 yr) radii of 12.3 ± 0.8 and -6.01 ± 0.2 mm for the anterior and posterior lens, respectively. While the differences are not statistically significant for the posterior lens, our anterior lens radii of curvature are significantly lower. Part of the difference might be due to differences in the age range of both groups. Our phakometry data are comparable with those reported by Garner and Smith[21] ($n=11$ with age ranging from 18 to 38 yr) with average lens radii of curvature of 11.54 ± 1.27 and -6.67 ± 0.97 mm for the anterior and posterior lens, respectively. Our data are also very consistent with recent reports using different methods. Manns *et al.*[38] measured phakometry *in vitro* on 13 pairs of unaccommodated human cadaver eyes and reported 10.15 ± 1.39 and -6.25 ± 0.79 mm for the anterior and posterior lens radii of curvature, respectively. Our phakometry data are also close to those of reports from distortion-corrected Scheimpflug images in subjects of similar age. Dubbleman and Van der Heijde's[27] empirical equation yields average anterior and posterior lens radii of 11.37 and -5.87 mm, respectively, for the average age of our subjects. Differences in the posterior lens are not significant. The slight differences in the anterior lens may be due to the fact that Scheimpflug cross sections are fitted to conic surfaces, and the apical radius is reported, while the Purkinje system samples more peripheral areas. Also, it should be noted that Scheimpflug images were captured with the subject viewing the fixation stimulus with the contralateral eye.

To our knowledge, the only data available in the literature on tilt and decentration of the crystalline lens are those reported by Kirschkamp *et al.*[26] and Dunne *et al.*[39] for the horizontal direction in two young groups. We report slightly higher values of crystalline lens tilt and larger intersubject variability (1.05 ± 1.12 deg for the horizontal direction and 0.77 ± 1.27 deg for the vertical direction) than those reported by Kirschkamp *et al.*[26] (0.2 ± 0.8 deg, horizontal direction) and Dunne *et al.*[39] (0.2 ± 1.8 deg, horizontal direction). We also found slightly higher decentrations (0.28 ± 0.12 mm for horizontal decentration and -0.06 ± 0.08 mm for vertical decentration as opposed to 0.1 ± 0.2 mm reported by Kirschkamp *et al.*[26] and -0.1 ± 0.1 mm reported by Dunne *et al.*[39]

Our measurements of IOL tilt and decentrations (0.87 ± 2.16 deg for horizontal tilt, 2.3 ± 2.33 deg for vertical tilt, and 0.25 ± 0.28 deg for horizontal decentration and -0.41 ± 0.39 mm for vertical decentration) can be compared with those of a few reports using Purkinje imaging or other methods. Those studies typically do not report the direction and sign of tilts and decentrations. Phillips *et al.*[17] used a Purkinje imaging system to measure tilt and decentration of posterior chamber IOLs in 13 patients and found average tilts of 7.8 ± 3 deg and decentrations of 0.7 ± 0.3 mm. While those estimates are larger than the ones obtained in our study, IOL designs and surgical techniques have evolved tremendously in the last 18 years, and the accuracy in lens positioning has potentially

improved. A more recent clinical study measured tilt and decentration after primary and secondary transsclerally sutured posterior chamber IOLs evaluating the Purkinje reflections while the subject was fixating at different locations in a Goldman perimeter.[40] This study reported an average IOL tilt of 5.71±3.41 deg in the first group (14 eyes) and 6.22±3.94 deg in the second group (42 eyes) and average decentrations of 0.67±0.43 and 0.59±0.43 mm, respectively. Those values are larger than those reported in the present study, potentially due to the surgical procedure and implicit assumptions in the methodology using perimetry. More recent studies used commercial Scheimpflug photography to assess tilt and decentration on different types of IOLs and found estimates very consistent with our results. One study[29] reported tilts and decentrations of polymethyl methacrylate (PMMA) and silicone IOLs in 70 eyes and found average tilts of 2.93±2.68 and 3.4±2.02 deg and average decentrations of 0.37±0.19 and 0.29±0.26 mm for the the PMMA and silicone groups, respectively). Another study[41] evaluated PMMA ($n=65$), three-piece silicone ($n=47$), and three-piece acrylic ($n=25$) IOLs and found average tilts of 2.67±0.84, 2.61±0.84, and 2.69±0.87 deg, respectively, and average decentrations of 0.31±0.15, 0.32±0.18, and 0.33±0.19 mm, respectively. The average estimates are very similar to those of our study. However, the intersubject variability, despite the larger sample of the Scheimpflug studies, seems excessively low.

A future study will address direct comparisons of phakometry as well as lens tilt and decentration with Purkinje and Scheimpflug imaging techniques on the same eyes.

B. Limitations of the Technique and Implication of the Results

We have developed a compact optical system to measure phakometry, and lens tilt and decentration, and demonstrated its use in both normal eyes and eyes with intraocular lenses (IOLs). Computer simulations have allowed us to test the methodology, the performance of the system, and the validity of the assumptions. We have shown that the equivalent mirror method tends to overestimate the posterior lens radius, very likely because light of the illuminating LEDs is not collimated, as suggested by Garner.[19] This configuration is not a limitation in the merit function procedure. The main limitation of the technique comes from the fact of considering spherical surfaces for the lens, which produces an overestimation of the lens radii of curvature. Although this limitation may be important in providing accurate phakometry measurements when larger asphericities are present, we have demonstrated that these differences do not affect tilt and decentration measurements. While this issue could be overcome by ensuring that the Purkinje images are formed in the apical zone, in general this is not practically possible, since for those angles the Purkinje images typically overlap. Other alternatives are the use of multiple double LEDs with different separations, which would allow estimates of radii of curvature as a function of radial distance and therefore estimates of asphericities, and the use of more sophisticated models for an equivalent mirror (or, better, for the merit function, since we have demonstrated that the latter gives more accurate phakometry) incorporating aspheric surfaces. The rest of the factors tested (gradient index of the lens, anterior chamber depth, lens thickness or corneal irregularities) do not seem to have a major impact on the measurements.

Although in most of the patients we could successfully measure phakometry, tilt, and decentration, there were several eyes with IOLs (not presented here) for which phakometry of the anterior lens was not possible, because the distance of the double PIII exceeded the pupil diameter. Presumably, these IOLs show very flat anterior surfaces. We have estimated that lenses with radii of curvature larger than 20 mm will produce that problem, with the current configuration of LED separation, and for a pupil size of 6 mm. Tilt and decentration measurements are possible, provided that nominal anterior radius is known and that tilt does not exceed 10 deg (for 0 mm decentration and for anterior lens radius of 10.45 mm).

While measurements of phakometry, tilt, and decentration of crystalline lenses/IOLs are informative for characterizing the normal eye or the outcomes of intraocular surgery, they will become particularly relevant, in combination with other optical and geometrical data, in modeling individual eyes and predicting their optical quality, in understanding the sources of aberrations, in shedding light on the mechanisms of accommodation, and in evaluating the potential benefits of different IOL designs.

ACKNOWLEDGMENTS

The authors acknowledge funding from Ministerio de Educación y Ciencia, Spain (grant BFM2002-02638) and Comunidad Autónoma de Madrid (grant GR/SAL/0387/2004) to Susana Marcos. Patricia Rosales acknowledges Ministerio de Educación y Ciencia for an FPI predoctoral fellowship. The authors also acknowledge Sergio Barbero, Lourdes Llorente, Sergio Ortiz, and Ignacio Jiménez-Alfaro for technical assistance and helpful discussions.

Author contact information: Instituto de Optica Daza de Valdes, C/Serrano 121, 28006, Madrid, Spain. Phone, 34-9-156-16800; fax, 3-49-156-45557; e-mail, Patricia@io.cfmac.csic.es, Susana@io.cfmac.csic.es.

REFERENCES

1. S. Marcos, S. A. Burns, P. M. Prieto, R. Navarro, and B. Baraibar, "Investigating sources of variability of monochromatic and transverse chromatic aberrations across eyes," Vision Res. **41**, 3861–3871 (2001).
2. F. J. Castejon-Mochon, N. Lopez-Gil, A. Benito, and P. Artal, "Ocular wavefront aberration statistics in a normal young population," Vision Res. **42**, 1611–1617 (2002).
3. J. McLellan, S. Marcos, and S. Burns, "Age-related changes in monochromatic wave aberrations in the human eye," Invest. Ophthalmol. Visual Sci. **42**, 1390–1395 (2001).
4. J. C. He, S. A. Burns, and S. Marcos, "Monochromatic aberrations in the accommodated human eye," Vision Res. **40**, 41–48 (2000).
5. L. Llorente, S. Barbero, D. Cano, C. Dorronsoro, and S. Marcos, "Myopic versus hyperopic eyes: axial length, corneal shape and optical aberrations," J. Vision **4**, 288–298 (2004).
6. E. Moreno-Barriuso, J. Merayo-Lloves, S. Marcos, R. Navarro, L. Llorente, and S. Barbero, "Ocular aberrations before and after myopic corneal refractive surgery: LASIK-

induced changes measured with laser ray tracing," Invest. Ophthalmol. Visual Sci. **42**, 1396–1403 (2001).
7. S. Barbero, S. Marcos, and I. Jimenez-Alfaro, "Optical aberrations of intraocular lenses measured *in vivo* and *in vitro*," J. Opt. Soc. Am. A **20**, 1841–1851 (2003).
8. C. Dorronsoro, S. Barbero, L. Llorente, and S. Marcos, "On-eye measurement of optical performance of rigid gas permeable contact lenses based on ocular and corneal aberrometry," Optom. Vision Sci. **80**, 115–125 (2003).
9. S. Marcos, S. A. Burns, E. Moreno-Barriuso, and R. Navarro, "A new approach to the study of ocular chromatic aberrations," Vision Res. **39**, 4309–4323 (1999).
10. S. Barbero, S. Marcos, and J. M. Merayo-Lloves, "Total and corneal aberrations in a unilateral aphakic subject," J. Cataract Refract. Surg. **28**, 1594–1600 (2002).
11. S. Marcos, S. Barbero, and I. Jiménez-Alfaro, "Optical quality and depth-of-field of eyes implanted with spherical and aspheric intraocular lenses," J. Cataract Refract. Surg. **21**, 223–235 (2004).
12. J. Wulfeck, "Infrared photography of the so-called third Purkinje image," J. Opt. Soc. Am. **45**, 928–931 (1955).
13. H. G. Van Veen and D. A. Goss, "Simplified system of Purkinje image photography for phakometry," Am. J. Optom. Physiol. Opt. **65**, 905–908 (1988).
14. A. Sorsby, B. Benjamin, and M. Sheridan, "Refraction and its components during the growth of the eye from the age of three," Spec. Rep. Ser. 301 (Medical Research Council, London, 1961).
15. D. Mutti, K. Zadnik, and A. Adams, "A video technique for phakometry of the human crystalline lens," Invest. Ophthalmol. Visual Sci. **33**, 1771–1782 (1992).
16. K. Zadnik, D. O. Mutti, G. L. Mitchell, L. A. Jones, D. Burr, and M. L. Moeschberger, "Normal eye growth in emmetropic schoolchildren," Optom. Vision Sci. **81**, 819–828 (2004).
17. P. Phillips, J. Perez-Emmanuelli, H. D. Rosskothen, and C. J. Koester, "Measurement of intraocular lens decentration and tilt *in vivo*," J. Cataract Refract. Surg. **14**, 129–135 (1988).
18. G. Smith and L. F. Garner, "Determination of the radius of curvature of the anterior lens surface from the Purkinje images," Ophthalmic Physiol. Opt. **16**, 135–143 (1996).
19. L. F. Garner, "Calculation of the radii of curvature of the crystalline lens surfaces," Ophthalmic Physiol. Opt. **17**, 75–80 (1997).
20. J. C. Barry, M. Dunne, and T. Kirschkamp, "Phakometric measurement of ocular surface radius of curvature and alignment: evaluation of method with physical model eyes," Ophthalmic Physiol. Opt. **21**, 450–460 (2001).
21. L. F. Garner and G. Smith, "Changes in equivalent and gradient refractive index of the crystalline lens with accommodation," Optom. Vision Sci. **74**, 114–119 (1997).
22. L. F. Garner and M. K. H. Yap, "Changes in ocular dimensions and refraction with accommodation," Ophthalmic Physiol. Opt. **17**, 12–17 (1997).
23. L. F. Garner, C. S. Ooi, and G. Smith, "Refractive index of the crystalline lens in young and aged eyes," Clin. Exp. Optom. **81**, 145–150 (1998).
24. D. L. Guyton, H. Uozato, and H. J. Wisnicki, "Rapid determination of intraocular lens tilt and decentration through the undilated pupil," Ophthalmology **97**, 1259–1264 (1990).
25. J. C. Barry, K. Branmann, and M. C. M. Dunne, "Catoptric properties of eyes with misaligned surfaces studied by exact ray tracing," Invest. Ophthalmol. Visual Sci. **38**, 1476–1484 (1997).
26. T. Kirschkamp, M. Dunne, and J. C. Barry, "Phakometric measurement of ocular surface radii of curvature, axial separations and alignment in relaxed and accommodated human eyes," Ophthalmic Physiol. Opt. **24**, 65–73 (2004).
27. M. Dubbelman and G. L. Van der Heijde, "The shape of the aging human lens: curvature, equivalent refractive index and the lens paradox," Vision Res. **41**, 1867–1877 (2001).
28. M. Dubbelman, G. L. Van der Heijde, and H. A. Weeber, "Change in shape of the aging human crystalline lens with accommodation," Vision Res. **45**, 117–132 (2005).
29. Wang Meng-Chi, Woung Lin-Chung, Hu Chao-Yu, and Kuo Han-Chin, "Position of poly(methyl methacrylate) and silicone intraocular lenses after phacoemulsification," J. Cataract Refract. Surg. **24**, 1652–1657 (1998).
30. M. Dubbelman, H. A. Weeber, R. G. L. van der Heijde, and H. J. Volker-Dieben, "Radius and asphericity of the posterior corneal surface determined by corrected Scheimpflug photography," Acta Ophthalmol. Scand. **80**, 379–383 (2002).
31. J. F. Koretz, S. A. Strenk, L. M. Strenk, and J. L. Semmlow, "Scheimpflug and high-resolution magnetic resonance imaging of the anterior segment: a comparative study," J. Opt. Soc. Am. A **21**, 346–354 (2004).
32. L. Llorente, S. Barbero, D. Cano, C. Dorronsoro, and S. Marcos, "Myopic versus hyperopic eyes: axial length, corneal shape and optical aberrations," J. Vision **4**, 288 (2004); http://journalofvision.org/4/4/5/.
33. L. F. Garner, H. Owens, M. K. H. Yap, M. J. Frith, and R. F. Kinnear, "Radius of curvature of the posterior surface of the cornea," Optom. Vision Sci. **74**, 496–498 (1997).
34. N. Sverker, P. Artal, P. Ann Piers, and V. D. Mooren, "Methods of obtaining ophthalmic lenses providing the eye with reduced aberrations," U. S. patent 6,609,793 (August 26, 2003).
35. M. Herzberger, "Colour correction in optical systems and a new dispersion formula," Opt. Acta **5**, 197-215 (1969).
36. T. Kirschkamp, M. Jockel, G. Wahlisch, and J. C. Barry, "Construction of a model eye to simulate Purkinje reflections for the determination of the radii of curvature and of the position of the crystalline lens of the eye," Biomed. Tech. **43**, 318–325 (1998).
37. J. C. Barry, A. Backes, and U. M. Pongs, "Corneal reflex distance from the limbus center is more accurate for the measurement of ocular misalignment than from the pupil center," Invest. Ophthalmol. Visual Sci. **38**, 531 (1997).
38. F. Manns, V. Fernandez, S. Zipper, S. Sandadi, M. Hamaoui, A. Ho, and J.-M. Parel, "Radius of curvature and asphericity of the anterior and posterior surface of human cadaver crystalline lenses," Exp. Eye Res. **78**, 39–51 (2004).
39. M. C. M. Dunne, L. N. Davies, E. A. H. Mallen, T. Kirschkamp, and J. C. Barry, "Non-invasive phakometric measurement of corneal and crystalline lens alignment in human eyes," Ophthalmic Physiol. Opt. **25**, 143–152 (2005).
40. D. Ismet, "Tilt and decentration after primary and secondary transsclerally sutured posterior chamber intraocular lens implantation," J. Cataract Refractive Surg. **27**, 227–232 (2000).
41. Jae Soon Kim and K. H. Shyn, "Biometry of 3 types of intraocular lenses using Scheimpflug photography," J. Cataract Refractive Surg. **27**, 533–536 (2001).